

STRUCTURAL, THERMAL AND OPTICAL PROPERTIES OF NOVEL OXYFLUOROTELLURIDE GLASSES

N. ELKHOSHKHANY^{a,b,*}, MAI MAHMOUD^a, EL SAYED YOUSEF^{c,d}

^a*Physics Dept., College of Arts and Sciences at Tabrjal, Jouf University, Al-Jouf, Saudi Arabia*

^b*Department of Material Science, Institute of Graduate Studies and Researches, Alexandria University, 163 Horreya Avenue, Shatby 21526, Egypt*

^c*Research Center for Advanced Materials Science (RCAMS), King Khalid University, Abha 61413, P. O. Box 9004, Saudi Arabia*

^d*Physics Dept., Faculty of Science, King Khalid University, P. O. Box 9004, Abha, Saudi Arabia*

Novel oxyfluorotellurite glasses within the composition $(80-x) \text{TeO}_2-10\text{P}_2\text{O}_5-10\text{ZnO}-x\text{NaF}$ in mol%, where $x = 0, 5, 7.5, 10, 12.5, 15, 20$ and 25 were prepared. The thermal kinetics and optical properties of these glasses were estimated by using differential scanning calorimetric (DSC), and UV-Vis-NIR spectroscopy respectively. The results of the thermal analysis were indicated that oxyfluorotellurite telluride glass has high thermal stability. The density, oxygen packing density, molar volumes, molar refraction, metallization criterion, molar polarizability, linear refractive index and optical basicity were calculated. It was found that with the increase NaF from TPZN0 0.0 to 15%, the linear refractive index (n) was increased otherwise the optical energy gap (E_{opt}) was decreased. The structure of the present glasses investigated by using infrared and Raman spectroscopy. Herein in this work, the results suggest that the present oxytelluride glasses modified by NaF can be used as a promising material in optical applications.

(Received March 16, 2019; Accepted June 4, 2019)

Keywords: Oxyfluoride tellurite glasses, Raman, Kinetic thermal analysis

1. Introduction

Tellurium and phosphorus oxide based glasses have been the topic of present researches as a result of its motivating optical, electrical and magnetic properties like high refractive index, high dielectric constant, low melting temperature, low glass transition temperatures, low viscosity, high thermal expansion, good infrared transmittance, visible wavelength and low phonon energy [1-5]. Thermal properties of Tellurite-phosphate oxide glasses have been studied at several papers, N. Mochida [6] have found that the thermal expansion coefficient decreases with increasing P_2O_5 content up to 28 mol% and the glass transition temperature increases. With more addition of P_2O_5 content leads to decrease of glass transition temperature and an increase of thermal expansion coefficient. Petr Mošner has studied thermal properties and stability of $\text{ZnO}-\text{P}_2\text{O}_5-\text{TeO}_2$ system [7]. Without a modifier such as alkali, alkaline earth oxide and other types of glass formers tellurium oxide down normal conditions does not have the ability to compose a glass so, the alkali metal such as (Na, Li, K) change the glass structure by giving rise to (NBOs) in the structure and effect on optical and thermal properties of the glass. The addition of alkaline earth oxides such as (ZnO, MgO, and CaO) improves glass forming nature [8-10]. In presence of glass modifier (ZnO) improves the mechanical properties, chemical and thermal resistivity, creates low rates of crystallization, decreases the melting temperature and increases the glass forming ability (promotes glass polymerization by creating chain-like structures of Te-O-Te) [11].

*Corresponding author: Elkhoshkhany@alexu.edu.eg

N. Elkhoshkhany had studied [31] the thermal stability of the glass system ($\text{TeO}_2\text{-ZnO-LiF-Nb}_2\text{O}_5\text{-NaF}$) and found that with increasing NaF content in glass system, the stability of glass was relatively large which provided a strong inhibition to the nucleation and the crystallization. The glass structure became more linked and hence required high thermal energy. It would be expected that the substitution of fluoride ions for oxide ions decreases the glass transition and deformation temperatures since two fluoride ions are substituted for an oxide ion, which causes the breakdown of the glass network structure. The water in the glasses may be controlled by introducing halides such as fluoride as the F^- substitution of OH^- groups [12-16].

The objective of this study is to examine the impact of adding NaF in the oxyfluoride glass network and explain their effects on the structure, physical, thermal and optical properties. This material may be used in several applications such as electrochemical and optoelectronics devices.

2. Experimental

The oxyfluoride telluride glasses of the following composition : $(80-x)\text{TeO}_2\text{-}10\text{P}_2\text{O}_5\text{-}10\text{ZnO-}x\text{NaF}$ with $x = (0, 5, 7.5, 10, 12.5, 15, 20, 25)$ were prepared by melt quench technique. All the starting chemicals were off 99.9% purity, (Sigma- Aldrich). Calculated weights of the chemicals were mixed in an agate mortar and melted in an electric furnace at $880\text{ }^\circ\text{C}$ for 30 min in a platinum crucible so that; a homogeneously mixed melt was obtained. The obtained melt was then quenched by pouring onto a preheated stainless steel mold to avoid excess thermal shocks. Directly after quenching, the glass (as-prepared sample) was annealed at $250\text{ }^\circ\text{C}$ for 1 hr in an annealing furnace, and then slowly cooled to the room temperature. The annealing process was performed to release the internal mechanical stresses to obtain the glass samples with good mechanical stability. The samples were then sliced into pieces with appropriate dimensions for the optical and density measurements.

2.2. Glass characterization

The amorphous nature of the glass samples was confirmed through (XRD) studies with a Philips X'Pert system. The density (ρ) was measured by the fluid displacement method depending on Archimedes principle. The (ρ) was calculated by using the relation (1). [17]

$$\rho_{\text{sample}} = \left(\frac{wt_{\text{air}}}{wt_{\text{air}} - wt_{\text{toluene}}} \right) * \rho_{\text{toluene}} \quad (1)$$

where wt_{air} is the weight of the glass sample in air and wt_{toluene} is the weight of the glass sample when immersed in toluene. The density of toluene = $0.864\text{ (g/cm}^3\text{)}$.

The molar volume (V_m) of the glass samples can be calculated using equation (2). [17]

$$V_m = \left(\frac{M_{wt}}{\rho_{\text{sample}}} \right) \quad (2)$$

where (M_{wt}) is the molecular weight of the sample.

The optical packing density (OPD) can be calculated using the relation (3):

$$\text{OPD} = \left(\frac{\rho * O}{M_{wt_{\text{sample}}}} \right) * 1000 \quad (3)$$

where, O is the number of oxygen atoms in each constituent oxide per formula unit.

2.2. Differential scanning calorimetry (DSC)

The characteristic temperatures of the samples were indicated by using a DSC (TA Instruments, SDT Q600). The DSC curves obtained at a temperature range ($250\text{ to }700\text{ }^\circ\text{C}$), at different heating rates (10, 15, 20, and $25\text{ }^\circ\text{K/min}$).

2.3. Optical absorption studies

In the visible and near ultraviolet regions optical absorptions were recorded at room temperature by using a double beam spectrophotometer (JASCO Corp, v-570, Rel -00 Japan) with a wavelength of range (200- 2500nm). A lapping machine with 600 grade and soft, fine AlO₃ powder was used in polishing the prepared glass samples. Opposite faces were finished optically flat and parallel with a high mirror-like surface, and a micrometre screw gauge with an accuracy of ± 0.01 mm was used to measure their thickness. A resolution limit of 0.2 nm and a sampling interval of 2 nm were utilized for the different 1150 measuring points.

2.4. (FTIR)

At room temperature the FTIR absorption spectra of the glasses were recorded by an FTIR system, type spectrum BX(PerkinElmer), using the KBr pellet technique at a wavenumber range of 500–1200 cm⁻¹, and resolution of 2 cm⁻¹.

2.5. Raman spectroscopy

The Raman absorption spectra of the glasses were recorded at room temperature using a wavelength 530nm, power 10nm, hole of laser entrance 25*1000 μ m, pulse duration 1sc, number of scan 2 and wide range (400to 4000).

3. Result and discussion

The prepared glass samples were homogeneous, light yellow, opaque and shiny with no air bubbles.

Table 1. Glass compositions and physical properties of glass system ((80-x) TeO₂-10P₂O₅-10ZnO-(x) NaF).

Samples name	Composition (mol%)	Density (ρ) (g/cm ³)	Molar volume (V _m) (cm ³ /mol)	OPD (g.atom/L)	Nb *10 ²² (cm-3)	\bar{F} (N. m-1)
TPZN0%	80TeO ₂ -10P ₂ O ₅ -10ZnO	5.193	28.89	76.15	8.75	241.7
TPZN5%	75TeO ₂ -10P ₂ O ₅ -10ZnO-5NaF	5.0961	28.28	60.0343	8.52	243.025
TPZN7.5%	72.5TeO ₂ -10P ₂ O ₅ -10ZnO-7.5NaF	4.9823	28.27	72.335	8.31	243.73
TPZN10%	70TeO ₂ -10P ₂ O ₅ -10ZnO-10NaF	4.9742	27.79	71.96	8.23	244.46
TPZN12.5%	62.5TeO ₂ -10P ₂ O ₅ -10ZnO-12.5NaF	4.9619	27.27	71.50	8.17	245.24
TPZN15%	65TeO ₂ -10P ₂ O ₅ -10ZnO-15NaF	4.8624	27.22	69.80	7.96	246.06
TPZN20%	60TeO ₂ -10P ₂ O ₅ -10ZnO-20NaF	4.842	26.12	68.91	7.84	247.85
TPZN25%	55TeO ₂ -10P ₂ O ₅ -10ZnO-25NaF	4.66	25.88	65.69	7.45	249.86

3.1. XRD, DSC and Thermal kinetics of TPZN glasses

XRD used to define the crystallinity and the structure of the material. The X-ray diffraction spectrum of prepared glass samples was shown in Fig. 1. The absences of sharp peaks in the XRD pattern confirm the amorphous nature of the sample structure.

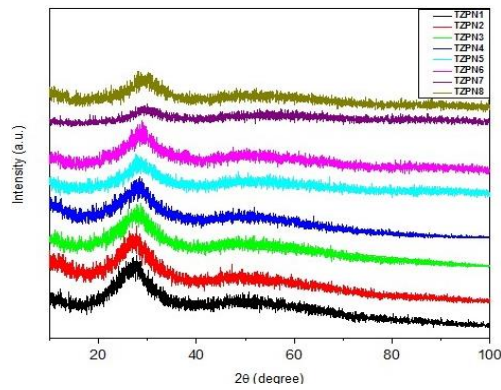


Fig. 1. XRD spectra of TPZN glass system.

Fig. 2 (a, b) showed the (DSC) profiles of TPZN7.5 and TPZN20% glass samples at different heating rate 10,15,20,25 K/min. Characteristic temperatures such as T_g , T_x , T_c and T_m were obtained from the DSC profiles are shown in Table 2.

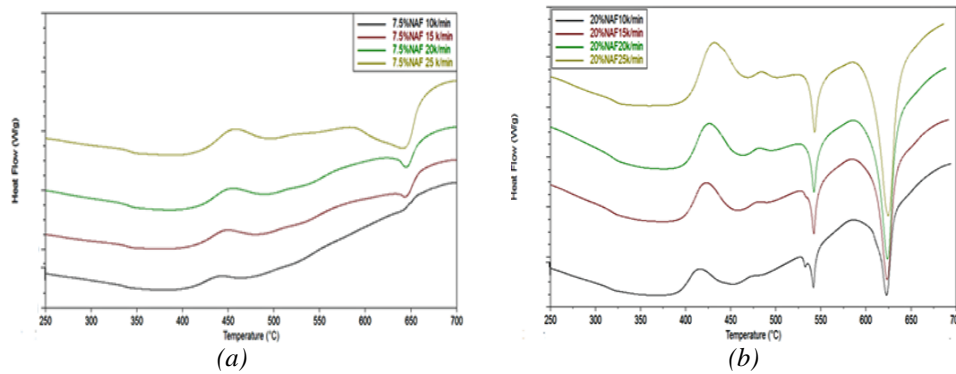


Fig. 2 (a, b). The (DSC) plot of TPZN7.5 and TPZN20% glass samples at heating rate $\alpha = 10, 15, 20, 25$ k/min.

Table 2. The glass transition temperature T_g , onset crystallization temperatures T_x , crystallization temperatures T_c , melting temperatures T_m , glass stability range S and glass factor K_g of (80-x) $TeO_2-10P_2O_5-10ZnO-xNaF$ glass system.

Glass name	T_g (k)	T_{x1} (k)	T_{c1} (k)	T_{x2} (k)	T_{c2} (k)	T_{m2} (k)	T_{m1} (k)	S_1	S_2	T_g/T_{m1}	T_g/T_{m2}	K_{g1}	K_{g2}
TPZN0%	615.8	696.59	755.5	---	---	---	900.17	80.79	---	0.68	---	0.97	---
TPZN5%	610.15	688.83	731.98	---	---	---	824.46	78.68	---	0.74	---	1.32	---
TPZN7.5%	605.61	689.29	721.98	---	---	---	916.62	80.68	---	0.66	---	0.59	---
TPZN12.5%	597.72	682.65	713.62	---	---	---	921.67	84.93	---	0.64	---	0.56	---
TPZN15%	597.77	688.72	717.86	---	---	---	892.32	90.95	---	0.67	---	0.41	---
TPZN20%	593.64	673.73	696.7	739.52	752.81	810.81	896.66	80.09	145.88	0.66	0.73	0.52	2.7
TPZN25%	588.66	679.92	709.34	744.15	759.2	815.38	890.99	91.26	155.45	0.66	0.72	0.66	3.04

Fig. 3 represented the DSC plot of the TPZN glass system at a heating rate $\alpha = 25$ K/min. Table 2 showed that the T_g values decreased from 615.8°C to 588.66°C with increasing in NaF(mol%).

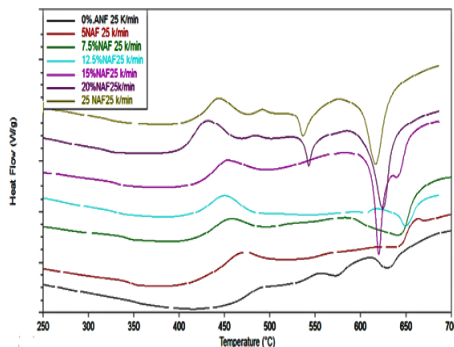


Fig. 3. The DSC plot of TPZN glass system at heating rate $\alpha=25$ K/min.

Decreasing in T_g values due to the replacement of TeO_2 by NaF creates some Te-F bonds and non-bridging fluorine ion with leads to weaker network structure. FTIR & Raman results confirmed the change of T_g where the decrease of TeO_4 units with the formation of TeO_{3+1} , TeO_3 (or) $\text{Te}(\text{O}, \text{F})_{3+1}$, $\text{Te}(\text{O}, \text{F})_3$ units. It was found that T_g is a function of both of (N_b and F) [18] where, N_b is the number of bonds per unit volume and F is the average stretching force constant. The number of bonds per unit volume of the glass N_b is calculated by Eq. (4):

$$N_b = \left(\frac{N_A}{V_m}\right) \sum(n_f x)_i \quad (4)$$

where N_A is Avogadro's number, V_m is the molar volume, x_i is the mole fraction and n_f is the coordination number of the oxide's cation in reference [18,20]. While the average stretching force constant F can be calculated by Eq. (5):

$$F = \frac{\sum(x n_f f)_i}{\sum(x n_f)_i} \quad (5)$$

where f is the stretching force constant founded in reference [6,20]. The values of N_b and F listed in Table 1. The values of N_b decreased from 8.75×10^{22} to $7.45 \times 10^{22} \text{ cm}^{-3}$ and F increased from 241.7 to 249.86 (N/m) and that's confirmed by the decreasing in T_g values in glass samples from TPZN0% to TPZN25% with increasing of NaF mol%. This glass system shows two crystallization temperature (T_{c1} , T_{c2}), two onset crystallization temperature (T_{x1} , T_{x2}) and two melting temperature (T_{m1} , T_{m2}) in glass samples TPZN20% and TPZN25%. The two crystallization temperature (T_{c1} , T_{c2}) represent the formation of two different crystalline phases, That confirmed the re-increased in values of the area under the curve in Raman results and changed in E_{opt} value in glass sample TPZN25% in UV results (Reconfiguration of bridging oxygen (BO) bridging Fluorine (BF)). Some useful parameters used for investigating devitrification and stability of the glass. These parameters are the glass stability S and the glass forming tendency K_g has shown in Table 2 which are given by the following equations [18,19]:

$$S = T_x - T_g \quad (6)$$

$$K_g = \frac{(T_c - T_g)}{(T_m - T_c)} \quad (7)$$

The glass stability S increases from 80.79 to 91.26°C and from 145.88 to 155.45°C, as shown in Table 2. This means that as NaF increases the stability of the glass increases.

For the studied glass compositions, the T_g/T_m values are listed in Table 2 all in the range from 0.64 to 0.74. This indicates that the prepared glasses have an excellent stability [21]. The

dependence of T_g on heating rate α can be determined from empirical relation shown by using the Eq. (8) [22]:

$$T_g = A + B \ln(\alpha) \tag{8}$$

where A and B are constants for a given glass composition. This dependence is shown in Fig. 4.

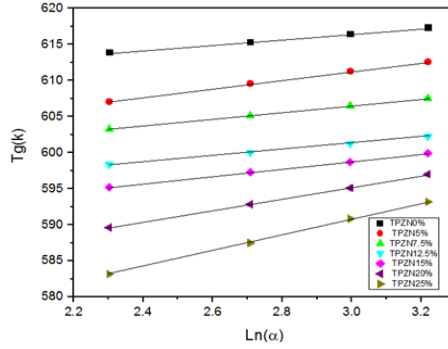


Fig. 4. Variation of T_g versus $\ln(\alpha)$ for TPZN glass system.

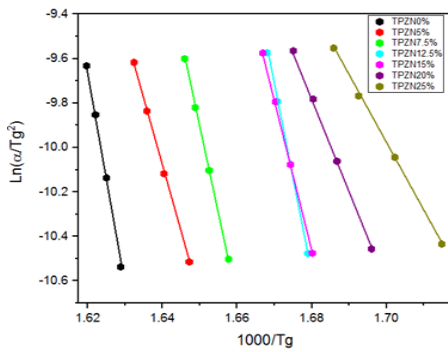


Fig. 5. Variation of $\ln(\alpha/T_g^2)$ versus $(1000/T_g)$ for TPZN glass system.

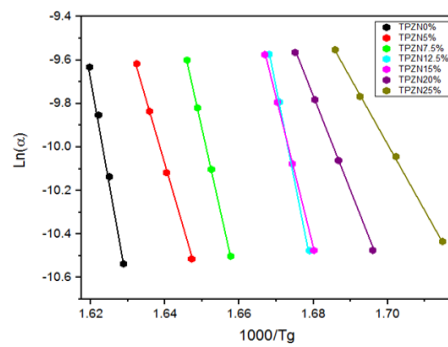


Fig. 6. Variation of $\ln(\alpha)$ versus $(1000/T_g)$ for TPZN glass system.

We apply Kissinger's formula stated by Eq. (18) [23] and Moynihan's formula stated by Eq. (19) [23] to obtain glass transition activation energy (E_g). E_g is obtained from a plot of $\ln(\alpha/T_g^2)$ versus $1000/T_g$ in Fig. 5 and a plot of $\ln(\alpha)$ versus $1000/T_g$ in Fig. 6 by taking the slopes of the resulting linear fits of data and listed in Table 3.

$$\ln\left(\frac{\alpha}{T_g^2}\right) = \left(\frac{-E_g}{RT_g}\right) + const \tag{9}$$

$$\ln \alpha = \left(\frac{-E_g}{RT_g} \right) + const \quad (10)$$

where R equal (8.314J/mol.K), the values of E_g changes from 789.863 to 344.865 KJ/mol by Kissinger's formula and from 795.17 to 360.27 KJ/mol by Moynihan's. The decreased in E_g is due to the formation of non-bridging oxygen's (NBO's) and non-bridging fluorine's (NBF's) [24] (weakness of the present glass structure) and due to decreasing in (n_b) as shown in Table 1 [20].

Here we used Kissinger's formula Eq. (20) [25] to obtain first and second crystallization activation energy E_{c1} and E_{c2} . E_{c1} and E_{c2} are obtained from a plot of $\ln(\alpha/T_{c1}^2)$ versus $1000/T_{c1}$ and a plot of $\ln(\alpha/T_{c2}^2)$ versus $1000/T_{c2}$ in Figs. 7, 8 respectively by taking the slopes of resulting linear fits of data. Data on E_{c1} and E_{c2} are listed in Table 3.

$$\ln \left(\frac{\alpha}{T_c^2} \right) = \left(\frac{-E_c}{RT_c} \right) + const \quad (11)$$

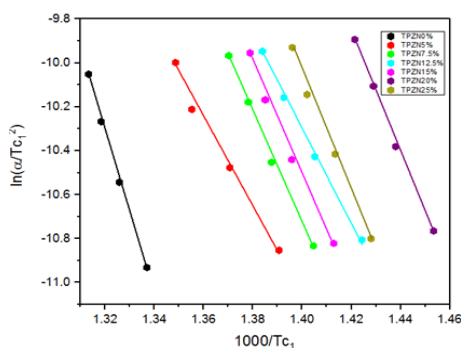


Fig. 7. Variation of $\ln(\alpha/T_{c1}^2)$ versus $1000/T_{c1}$ for TPZN glass system.

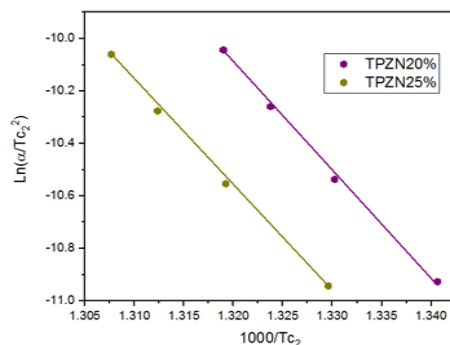


Fig. 8. Variation of $\ln(\alpha/T_{c2}^2)$ versus $1000/T_{c2}$ for TPZN glass system.

Table 3. The transition activation energy E_t and the crystallization activation energy E_c for TPZN glass system.

Glass name	E_g (kJ/mol)	E_g (kJ/mol)	E_{c1} (kJ/mol)	E_{c1} (kJ/mol)	E_{c2} (kJ/mol)	E_{c2} (kJ/mol)
TPZN0%	789.863	795.17	311.52	315.1	---	---
TPZN5%	496.67	486.78	320.27	181.96	---	---
TPZN7.5%	652.32	634.32	211.75	229.02	---	---
TPZN12.5%	708.02	719.83	180.75	189.64	---	---
TPZN15%	559.53	571.01	215.32	299.63	---	---
TPZN20%	344.865	360.27	288.63	244.432	353.01	344.02
TPZN25%	253.411	253.35	288.87	244.76	352.68	335.38

Also, E_c can be calculated from Ozawa and Chen according to Eq. (12) [25] and the data listed in Table 3.

$$\ln(\alpha) = \left(\frac{-E_c}{RT_c}\right) + const \quad (12)$$

Here, E_{c1} , E_{c2} are obtained from a plot of $\ln(\alpha)$ versus $1000/T_{c1}$ and a plot of $\ln(\alpha)$ versus $1000/T_{c2}$ in Figs. 9, 10 respectively by taking the slope of the resulting linear fits of data.

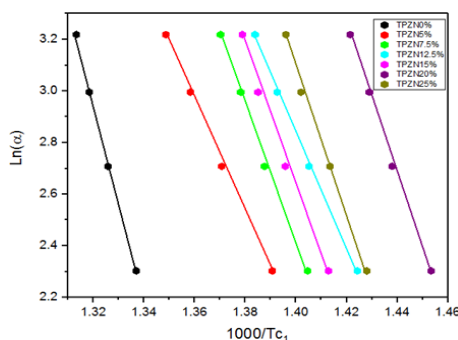


Fig. 9. Variation of $\ln(\alpha)$ versus $1000/T_{c1}$ for TPZN glass system.

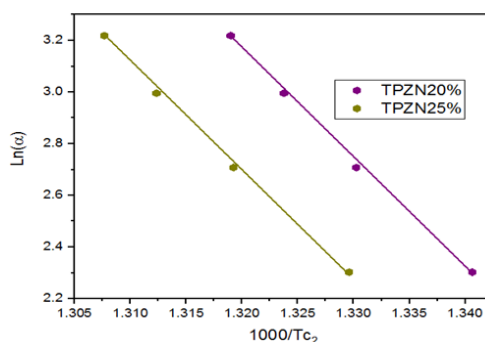


Fig. 10. Variation of $\ln(\alpha)$ versus $1000/T_{c2}$ for TPZN glass system.

The values of E_{c1} decrease from 311.22 to 288.87 KJ/mol and the values of E_{c2} decrease from 353.01 to 325.68 KJ/mol by Kissinger's formula, while E_{c1} decreases from 315.1 to 244.76 KJ/mol and E_{c2} decreases from 344.02 to 335.38 KJ/mol by applying Ozawa and Chen. The decrease in E_c values indicates decreasing the energy barrier required for the crystallization with the increasing NaF content [25].

3.2. Density, molar volume and Oxygen packing density

The (ρ), (V_m) and (O.P.D) of the glass samples are given in Table 1. The density, molar volume and (O.P.D) values decrease with increasing NaF mol% and decreasing TeO_2 mol%. It is seen from Fig. 11 that, the density decreases from 5.193 to 4.66 g/cm^3 with the addition of NaF to TeO_2 glass network and this can be due to the substitution of lower molecular weight of alkali halide (NaF) (41.98817g/mol) instead of higher molecular weight of TeO_2 (159.5988 g/mol).

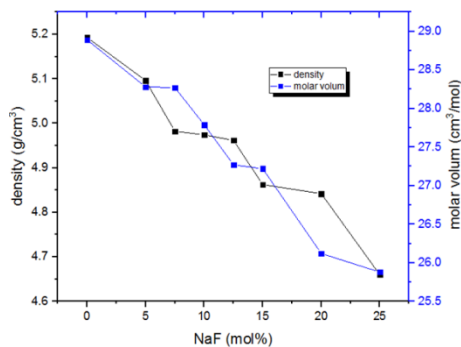


Fig. 11. Variation of density and molar volume with NaF mol% in TPZN glass system.

So, the glass matrix became less dense because the substitution of TeO_2 by NaF (fluoride atoms replaced the oxygen atoms). Also, the (V_m) of the present glasses decreases from 28.89 to 25.88 (cm^3/mol) when increasing NaF content. The decrease in V_m could be related to the decrease in inter-atomic spacing and bond length of Na-F [26]. Where fluorine is a small atom with a large electronegativity since the radius of F^- smaller than the radius of O^{2-} . From Table 1 it is found that OPD decreases from 76.15 to 65.69 (mol/L) when NaF is substituted by TeO_2 and in turn, the decrease in OPD is ascribed to decrease in the number of oxygen.

3.3. Optical properties

3.3.1. Determination of the optical band gap (E_{opt}) and Urbach energy (ΔE):

E_{opt} : energy gap between the valence band and conduction band can be determined by using Davis's and Mott's relation (13) [27-29]

$$\alpha h\nu = A(h\nu - E_{\text{opt}})^n \quad (13)$$

where A is a constant, n is an index has values 1/2, 3/2, 2, 3 depending on the nature of the transition, $\alpha(\nu)$ is the absorption coefficient and ($h\nu$) is photon energy of incident radiation. E_{opt} obtained by extrapolating the absorption coefficient to zero absorption in the plot of $(\alpha h\nu)^{1/2}$ versus ($h\nu$) as shown in Fig. 12. The values of E_{opt} are listed in Table 4. The optical band gap (E_{opt}) decreased from 3.25 to 2.71 in TPZN0% to TPZN15% glass samples and back increased from 2.71 to 3.22 in TPZN15% to TPZN25% glass samples. The decreased in (E_{opt}) values were due to the addition of modifier such as alkali (Na) which break BOs and created NBOs [30] in breakage of the glass network since the bridging oxygen less excited than non-bridging oxygen [30]. The Re-increases in (E_{opt}) values because of the effect of F^- ion on Te-O bonds in tellurite glass network. Where reconstitution occurs in the composition of the bridging the resulted confirm what happened in Raman absorption.

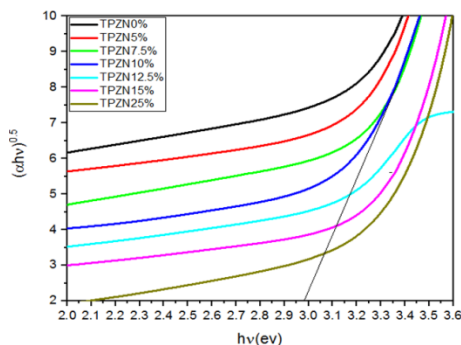


Fig. 12. Plot of $(\alpha h\nu)^{1/2}$ versus ($h\nu$) for TPZN glass system.

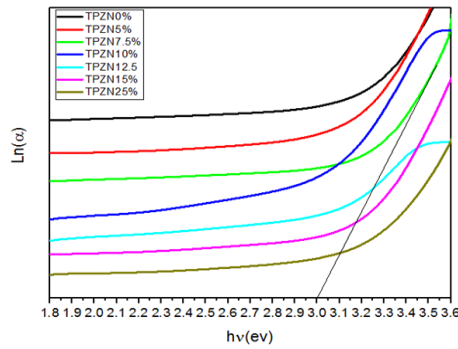


Fig. 13. Plot of $\ln(\alpha)$ versus $(\hbar\nu)$ for TPZN glass system.

Urbach energy (ΔE): the width of band tails of localized states (ΔE) were calculated from the slope of the linear regions of the plots $\ln(\alpha)$ against $(\hbar\nu)$ as shown in the Fig. 13 and correspond to the expression (14) [31,32].

$$\ln \alpha = \left(\frac{\hbar\nu}{\Delta E} \right) - C \quad (14)$$

(ΔE) decreases from 0.246 to 0.184 eV with increasing of NaF content as listed in Table 4. The decreasing of (ΔE) values refer to the present glass system is highly stable and homogenous.

3.3.2. Determination of refractive index (n), Molar refractivity (R_m), metallization criterion (M) and electronic polarizability (α_m)

We are calculated the (n) from the relation (15) [33,34].

$$\frac{(n^2+1)}{(n^2-1)} = 1 - \sqrt{\frac{E_{opt}}{20}} \quad (15)$$

We observed that the value of n increases from 1.99 to 2.106 with increasing NaF from 0 to 15mol% listed in Table 4 due to increasing in polarizability (non-bridging oxygen) and decreasing in density.

Table 4. refractive index n , Molar refraction R_m , metallization criterion M , electronic polarizability of the material α_m , electronic polarizability of the oxide ion α_o^{2-} , optical basicity A , thickness (d), optical energy gap (E_{opt}) and Urbach energy (ΔE) of $((80-x)TeO_2-10ZnO-10P_2O_5-xNaF)$ glass system.

Sample code	n	R_m	M	$\alpha_m/10^{-24}$	α_o^{2-}	A	d	E_{opt}	ΔE
TPZN0%	1.99	14.35	0.503	5.69	2.188	0.91	0.225	3.25	0.246
TPZN5%	1.994	14.1	0.501	5.595	2.264	0.93	0.23	3.24	0.247
TPZN7.5%	1.997	14.13	0.501	5.595	2.35	0.96	0.21	3.22	0.236
TPZN10%	2.04	14.26	0.485	5.67	2.447	0.99	0.22	2.99	0.226
TPZN12.5%	2.103	14.54	0.467	5.77	2.564	1.02	0.23	2.72	0.196
TPZN15%	2.106	14.53	0.466	5.77	2.65	1.04	0.285	2.71	0.196
TPZN25%	1.997	12.91	0.501	5.12	2.66	1.042	0.265	3.22	0.184

Then the value of n decreases from 2.016 to 1.997 with increasing NaF from 15 to 25 mol% due to decreased in polarizability as a result of re-configuration bridging. (R_m) calculated by using Eq (16) [34].

$$R_m = \left[\frac{(n^2-1)}{(n^2+2)} \right] V_m \quad (\text{cm}^3/\text{mol}) \quad (16)$$

The values of R_m decrease from 14.35 to 12.91 (cm^3/mol) listed in Table 4 with the increasing of NaF from 0 mol% to 25mol% with the decreasing of TeO_2 due to decreases of molar volume (V_m).

(M) calculated to investigate the insulting behaviour of glass samples. The glass samples lay within the range of (0.468–0.507) listed in Table 4 were calculated from Eq (17) [31]

$$M = 1 - \left(\frac{R_m}{V_m} \right) \quad (17)$$

where the most of tellurite glasses exist in the range 0.35–0.45 [34]. Electronic polarizability calculated by using the relation (18) [31].

$$\alpha_m = \left(\frac{3}{4\pi N} \right) R_m \quad (\text{cm}^3) \quad (18)$$

The value of α_m decreases from 5.69 to 5.12 cm^3 listed in Table 4 by increasing of NaF and decreasing TeO_2 due to the decreasing number of non-bridging oxygen in the glass system where non-bridging oxygen (NBO) have a high tendency to polarize compared with bridging-oxygen (BO).

3.3.3. Determination of optical basicity from the electronic polarizability of oxygen ion (α_o^{2-})

The (α_o^{2-}) was calculated by using Eq (19) [35].

$$\alpha_o^{2-}(E_g) = \left[\left(\frac{V_m}{2.52} \right) \left(1 - \sqrt{\frac{E_g}{20}} \right) - \sum \alpha_i \right] (N_o^{2-})^{-1} \quad (\text{\AA}^3) \quad (19)$$

where $\alpha_o^{2-}(E_g)$ energy band gap based oxide ion polarizability, α_i molar cation polarizability and N_o^{2-} denotes the number of oxide ions in the chemical formula A_pO_q . The molar cation polarizability values of Te^{4+} , Zn^{2+} and P^{5+} ions are respectively $\alpha_i \text{Te} = 1.595 \text{\AA}^3$, $\alpha_i \text{Zn} = 0.283 \text{\AA}^3$ and $\alpha_i \text{P} = 3.63 \text{\AA}^3$. The calculated values of $\alpha_o^{2-}(E_g)$ are tabulated in Table 4.

The optical basicity (Λ) was calculated using the Eq (20) [35].

$$\Lambda = 1.67 \left[1 - \left(\frac{1}{\alpha_o^{2-}} \right) \right] \quad (20)$$

Our calculation in Table 4 clarified that the Λ decreases with decreasing of (α_o^{2-}) so, the relation between them was a direct correlation due to the addition of NaF content instead of TeO_2 content.

3.4. Structure of TPZN glasses

3.4.1. Fourier transforms infrared spectroscopy (FTIR)

When the samples undergo infrared spectroscopy, molecules that form bonds will absorb specific frequencies to rotate and vibrates in glass system. The FTIR spectra of the prepared glass sample given in Fig. 14 with a range of (400 – 4400 cm^{-1}). Looking at Fig. 14 the absorption spectra of the glass samples contains of two strong, broad absorption bands around 624 cm^{-1} and 1046 cm^{-1} , one weak, broad absorption band around 440 cm^{-1} , and two mediate peaks around 3440 cm^{-1} , 908 cm^{-1} and two shoulders around 770 cm^{-1} and 1170 cm^{-1} for all glasses. The band around 624 cm^{-1} is assigned to The vibration of oxygen atoms in P-O-P bridges in metaphosphate Q^2 [36,45]. The band around 1064 cm^{-1} is assigned to asymmetric vibration of (PO_3) $^{2-}$ [37,45]. The band around 440 cm^{-1} is due to Zn-O linkages [38]. The mediate peak around 3440 cm^{-1} is attributed to stretching mode of strong hydrogen bonded Te-OH groups [39,40]. The another mediate peak

908cm^{-1} is assigned to the symmetric vibration of $(\text{PO}_3)^{2-}$ [41]. The shoulder around 770 can be attributed to Symmetrical vibration of TeO_{eq} bonds of TeO_4 units [42]. The other shoulder around 1170 is assigned to the symmetric vibration of $(\text{PO}_2)^-$ [43,45]. The deconvoluted IR spectra of TPZN0% and TPZN25% glasses by using a Gaussian function is shown in Fig. 15 which were symbolized as (1-20) bands and the assignments of each peak are recorded in Table 5. In our study in samples TPZN0% and TPZN25% with the addition of NaF to TeO_2 glasses of broad absorption bands 8 and 12 shifted towards lower wavenumber and O^{2-} bridging Te^{4+} replaced by F^- due to the same ionic radii of F^- and O^{2-} . The result of the impact of F^- in Te-O-Te linkages in the glass matrix transforms TeO_4 to TeO_{3+1} and TeO_3 or $\text{Te}(\text{O}, \text{F})_{3+1}$ and $\text{Te}(\text{O}, \text{F})_3$ decreasing the connectivity of the tellurite glass former network. Also, by adding NaF to TeO_2 glass the peak number 10 and 13 shifted towards a higher wave number by increasing NaF due to the appearance of TeO_3 units with a reduction in the number of TeO_4 units. Consequently, the addition of NaF reduces Te-O-Te linkages due to gradually transformation of trigonal bipyramid TeO_4 and $\text{Te}(\text{O}, \text{F})_4$ through TeO_{3+1} and $\text{Te}(\text{O}, \text{F})_{3+1}$ to trigonal pyramid TeO_3 and $\text{Te}(\text{O}, \text{F})_3$ with increasing NaF. The FTIR investigation of Fluoro-tellurite crystalline found that two oxyfluoride phases TeO_3F_2 and TeOF_2 according to the formation of α and β - TeO_2 polymorphs, respectively [31].

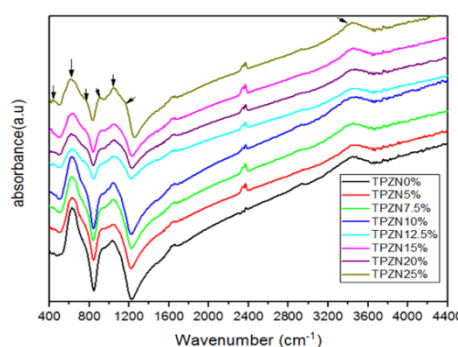


Fig. 14. FTIR spectra of TPZN glass system.

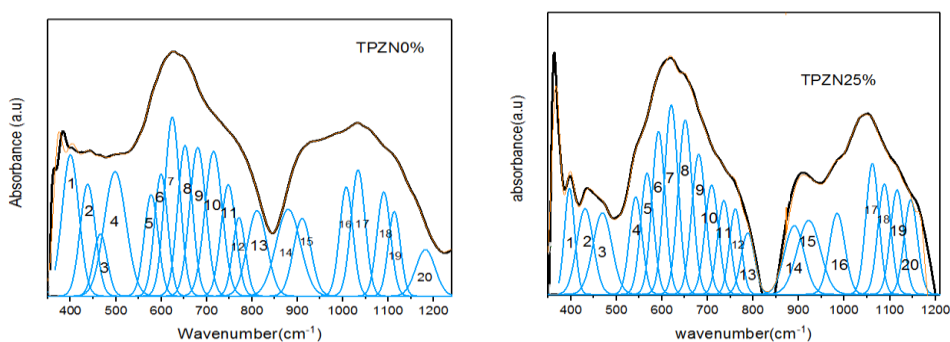


Fig. 15. De-deconvoluted FTIR spectra of TPZN glass system.

Table 5. Assignment of FTIR bands of the glass system $((80-x) \text{TeO}_2-10\text{P}_2\text{O}_5-10\text{ZnO}-(x) \text{NaF})$.

Peak number	Peak positions cm^{-1}		Assignments
	TPZN0%	TPZN25%	
1	389	390	Bending vibrations of phosphate [36,45]
2	435	432	Vibrations of Zn-O bonds from ZnO_4 groups [42]
3	464	467	Symmetrical stretching or bending vibrations of Te-O-Te linkages [42]
4	500	547	Deformation vibration mode of P-O ⁻ [43]
5	575	568	Symmetric and asymmetric stretching and bending vibrates of (TeO_{3+1}) linkages [37]
6	599	594	Vibration of the continuous network consisting of TeO_4 tbp [44]
7	627	622	The vibration of oxygen atoms in P-O-P bridges between metaphosphate Q^2 and diphosphate Q^1 units [45]
11	745	740	
8	654	647	Axial asymmetric stretching vibrations of (Te-O) of tetrahedral TeO_4 units [42]
9	677	680	Symmetric vibration of P-O-P [45]
10	710	714	Symmetric stretching vibrations of TeO_3 units [44]
12	772	763	Symmetrical vibration of TeO_{eq} bonds of TeO_4 units [42]
13	795	815	(Te-O) symmetric & (Te-O) asymmetric vibration modes of TeO_3 [44]
14	881	892	Asymmetric vibration of (P-O-P) [43]
15	911	917	Symmetric vibration of $(\text{PO}_4)^{3-}$ [43]
16	1006	1012	Symmetric vibration of $(\text{PO}_3)^{2-}$ [43]
17	1034	1038	Symmetric vibration of $(\text{P}_2\text{O}_7)^{4-}$ [43]
18	1092	1090	Asymmetric vibration of $(\text{PO}_3)^{2-}$ [43]
19	1114	1118	Symmetric vibration of $(\text{PO}_2)^-$ [43]
20	1182	1178	Asymmetric vibration of $(\text{PO}_2)^-$ [43]

3.4.2. Raman spectra

The Raman spectra of studying glasses are shown in Fig. 16. Four modes describe all the glasses: two strong peaks around 468, 666, one shoulder around 780 and one weak peak around 1024.

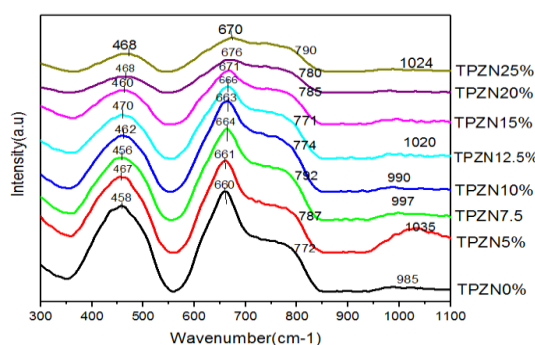


Fig. 16. Raman spectra of TPZN glass system.

All the spectra are deconvoluted using Gaussian fitting to measure accurate Raman peak positions and are shown in Fig. 17 which were symbolized as (a-p) bands. The positions of the Raman bands of these glasses and their assigned vibrational modes are listed in Table 6. In Fig. 17 showed the band (a) at $(409-425) \text{cm}^{-1}$ is assigned to TeO_3 tps units with two or three nonbridging oxygen [31]. Band (b) at $(430-452) \text{cm}^{-1}$ is assigned to bending vibrations of phosphate units [41]. Broad Raman band (c) at $(449-471) \text{cm}^{-1}$ is given to ZnO_4 structural units [42]. Band (d) at $(474-488) \text{cm}^{-1}$ is given to stretching and bending vibrations of Te-O-Te linkages in TeO_4 (tbps), TeO_{3+1} polyhedral and TeO_3 (tps) [42] due to the transference of TeO_4 groups into TeO_3 groups. A The band (e) at $(498-506) \text{cm}^{-1}$ is given to deformation, the vibration mode of P-O⁻ [43]. The band (E) at $(591-619) \text{cm}^{-1}$ is assigned to symmetric and asymmetric stretching and bending vibrate of (TeO_{3+1}) linkages [37]. The band (f) at $(612-637) \text{cm}^{-1}$ is assigned to vibration of the continuous

network consisting of TeO_4 tbp [44]. The band (h) of $(648-662) \text{ cm}^{-1}$ is assigned to symmetrical stretching vibrational modes of $(\text{Te}_{\text{ax}}-\text{O})_s$ of TeO_4 units [28]. The band (j) at $(688-702) \text{ cm}^{-1}$ and band (p) at $(794-816) \text{ cm}^{-1}$ is assigned to the symmetric and asymmetric vibration of P-O-P [36]. The band (K) at $(704-721) \text{ cm}^{-1}$ assigned to stretching modes of nonbridging oxygen (NBO) found on the TeO_3 [44]. The peak (g) at $(632-643) \text{ cm}^{-1}$ and peak (m) at $(740-758) \text{ cm}^{-1}$ are given to vibration of oxygen atoms in P-O-P bridges in diphosphate atoms Q^1 unit and metaphosphate atoms [43]. The peak (n) at $(758-775) \text{ cm}^{-1}$ is assigned to $(\text{Te}_{\text{eq}}-\text{O})_s$ and $(\text{Te}_{\text{eq}}-\text{O})_{\text{as}}$ vibrational modes of TeO_4 [28]. The band (O) at $(775-792) \text{ cm}^{-1}$ assigned to $(\text{Te}-\text{O})$ symmetric & $(\text{Te}-\text{O})$ asymmetric vibration modes of TeO_3 [44]. In our study, we spotted changes in the Raman spectra of glasses with the adding NaF content. By adding NaF to TeO_2 glasses occurs substitution of fluoride ions (higher electronegativity) for oxide ions, and as two fluoride ions would take the place of one oxide ion. As a result, the breakdown of the glass network structure occurs. As the fluoride (NaF) content increases, the peak (d) minimizes and shifts from lower wavenumber to higher wavenumber $(474 \text{ to } 488) \text{ cm}^{-1}$ indicating that the vibrations of the Te-O-Te linkage in these samples are due to the transformation of TeO_4 groups into TeO_3 groups. The intensities of Peaks (h) and (n) decreased in (TPZN0%-TPZN15%) and, increased in (TPZN20%, TPZN25%) and then, they shifted towards higher wave numbers $(\text{from } 648 \text{ to } 662) \text{ cm}^{-1}$ and $(\text{from } 758 \text{ to } 775) \text{ cm}^{-1}$ respectively. It is ascribed to the decrease of TeO_4 units and F^- breaks Te-O-Te linkages in the glassy network with the formation of TeO_{3+1} , TeO_3 or/and $\text{Te}(\text{O}, \text{F})_{3+1}$, $\text{Te}(\text{O}, \text{F})_3$ units in oxyfluoride tellurite glasses. Causes changes in the glass structure and the connectivity of the tellurite former network. The increase in the intensity of the peak (i) and peak (l) in (TPZN5% to TPZN25%) around $(652-673) \text{ cm}^{-1}$ and $(728-766) \text{ cm}^{-1}$ were due to the reconfiguration of oxygen bridging (BO) or fluorine bridging (BF) by adding fluoride ions which replace bridging oxide ions in the TeO_4 that becomes $\text{Te}(\text{O}, \text{F})_4$. The chain structure will stabilize when two TeO_4 are linked by the BF ion and then $\text{Te}(\text{O}, \text{F})_4$ turn into $\text{Te}(\text{O}, \text{F})_3$ with the increase of NaF. The fraction ratio values of intensities of $\text{TeO}_4 / (\text{TeO}_4 + \text{TeO}_3)$ are 0.63, 0.61, 0.61, 0.59, 0.58, 0.57, 0.61 and 0.62 respectively; with increasing concentration of NaF from 0 to 25 mol%. The decrease in values of fraction ratio show that more non bridging oxygen's (NBO), and the increase in values in (TPZN20% and TPZN25%) confirm the re-configuration of (BO) and (BF) so, TeO_4 becomes $\text{Te}(\text{O}, \text{F})_4$ with bridging fluoride (BF) ions as a result of the stronger hetero-Polar bond strength of fluoride ion than oxygen ion. This BF ion will stabilize chain structure when two TeO_4 are connected by the BF ion, so the $\text{Te}(\text{O}, \text{F})_4 / \text{Te}(\text{O}, \text{F})_3$ ratio becomes higher with increasing fluoride content.

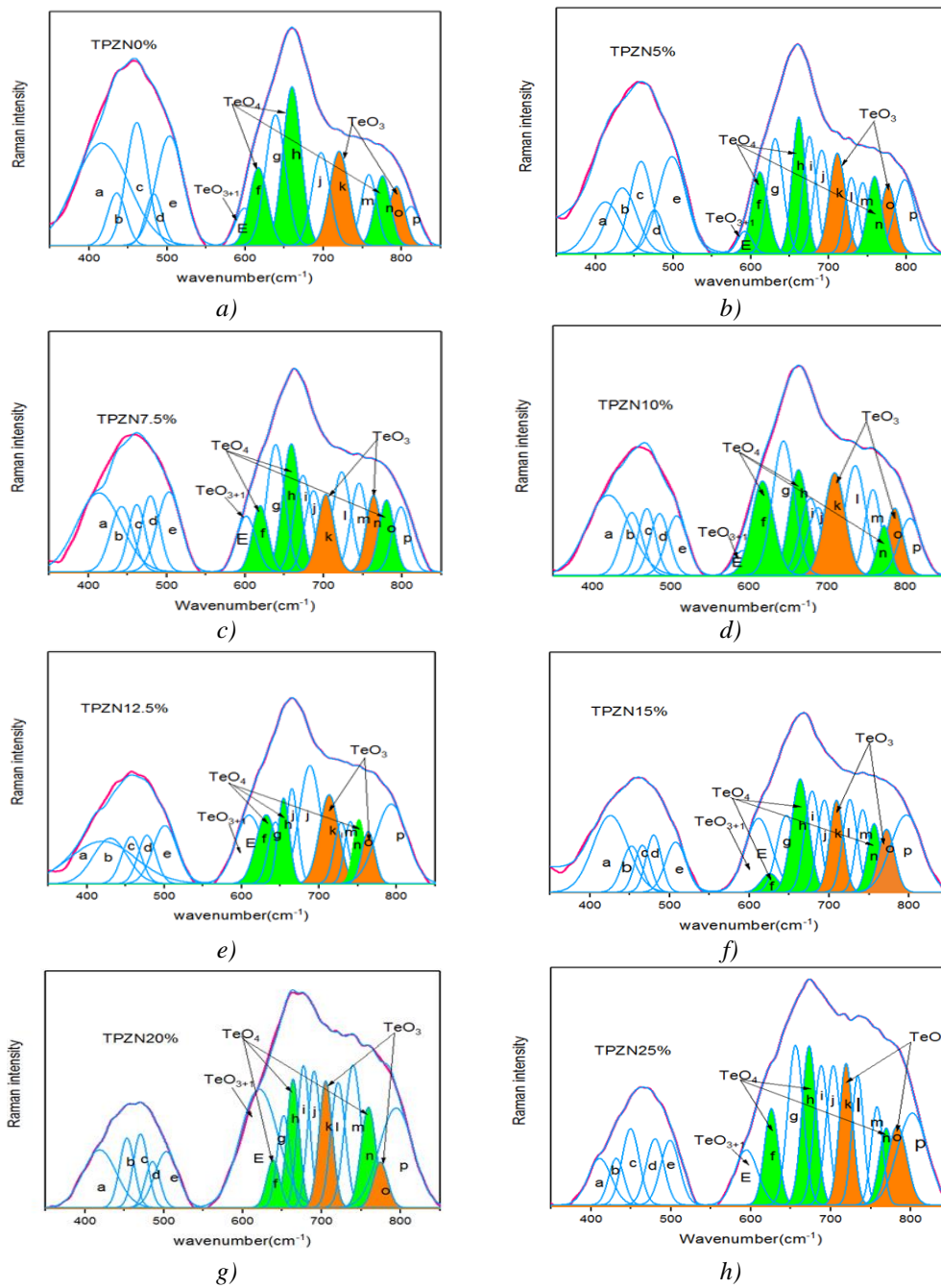


Fig. 17. De-convoluted Raman spectra of TPZN glass system at different concentrations: a) 0%; b) 5%; c) 7,5%; d) 10%; e) 12,5%; f) 15%; g) 20%; h) 25%

Table 6. Raman bands of $\text{TeO}_2\text{-ZnO-P}_2\text{O}_5\text{-NaF}$ glasses.

symbol	observed Raman bands in the glass (cm^{-1})	Raman assignments
a	409 - 425	TeO_3 tps units with two or three nonbridging oxygen
b	430 - 452	Bending vibrations of phosphate units
c	449 - 471	ZnO_4 tetrahedral group
d	474 - 488	Symmetrical stretching or bending vibrations of Te-O-Te linkages
e	498 - 506	Vibrations of PO_4 units
E	591 - 619	Symmetric and asymmetric stretching and bending vibrates of (TeO_{3+1}) linkages
f	612 - 637	Vibration of the continuous network consisting of TeO_4 tbp
g	632 - 643	Vibration of oxygen atoms in P-O-P bridges in meta phosphate atoms Q^2 unit
h	648 - 662	Symmetrical vibration of TeO_{ax} bonds of TeO_4 units
i	662 - 687	(O-Te-O) linkages are replaced by(O-Te-F)
j	688 - 702	Symmetric vibration of (P-O-P)
k	704 - 721	Stretching modes of nonbridging oxygen (NBO) found on the TeO_3
l	721 - 736	(Te-O) symmetric & (Te-O) asymmetric vibration modes of $\text{Te}(\text{O},\text{F})_3$ units
m	740 - 758	Vibration of oxygen atoms in P-O-P bridges in di phosphate atoms Q^1 unit
n	758 - 775	Symmetrical vibration of TeO_{eq} bonds of TeO_4 units
o	775 - 792	(Te-O) symmetric & (Te-O) asymmetric vibration modes of TeO_3
P	794 - 816	Asymmetric vibration of (P-O-P)

4. Conclusions

Synthesis of new oxyfluoride tellurite glasses $[(80-x)\text{TeO}_2-10\text{ZnO}-10\text{P}_2\text{O}_5-x\text{NaF}]$ where $x=0, 5, 7.5, 10, 12.5, 15, 20$ and 25 mol% were prepared. From (XRD), the amorphous nature of the glass samples was observed. The ρ , V_m and n_b were decreased by increasing of NaF content instead of the TeO_2 content, while the \bar{r} increased. The result from FTIR and Raman spectra, observed that, in the present glass system the fluorine ions (F^-) substituted oxygen ions (O^{2-}) in TeO_4 units resulting in the formation of (BF) units and the conversion of $\text{Te}(\text{O}, \text{F})_4$ units into $\text{Te}(\text{O}, \text{F})_3$ units through $\text{Te}(\text{O}, \text{F})_{3+1}$ with the increase of NaF content. The ratio of $\text{TeO}_4/(\text{TeO}_4+\text{TeO}_3)$ decreased from 0mol% to 15mol% and then increased in 20mol% and 25mol%. Band gap (E_{opt}) decreased and then increased in 25 mol% with increasing of NaF content. The R_m , M , and α_m decreased, but the α_o^{2-} and Λ of the glass increased. From DSC T_g decreased because of weakness in the glass structure due to the formation of (NBF) and (NBO).

Acknowledgements

One of the authors, N. Elkhoshkhany, wishes to thank Professor M. Elsherbiny, Department of Material Science, Institute of Graduate Studies and Researches, Alexandria University, Egypt, for cooperation, interest in this work and helpful.

The authors extend their appreciation to the Deanship of Scientific Research at King Khalid University (KKU) for funding this research project Number (R.G. P2. /22/40).

References

- [1] H. H. Hegazy, Samar Almojadah, M. Reben, Optics & Laser Technology **74**, 138 (2015).
- [2] Raffaella Rolli, Karl Gatterer, Mario Wachtler, Marco Bettinelli, Adolfo Speghini, David Ajo, Spectrochimica Acta Part A: Molecular and Biomolecular Spectroscopy **57**(10), 2009 (2001).
- [3] Jian Lin, Wenhai Huang, Zhengrong Sun, Chandra S. Ray, Delbert E. Day, J. Non-Cryst. Solids **336**(3), 189 (2004).

- [4] H. A. A. Sidek, S. Rosmawati, Z. A. Talib, M. K. Halimah, W. M. Daud, *Am. J. Appl. Sci.* **6**(8), 1489 (2009).
- [5] Marvin J. Weber, John D. Myers, Douglas H. Blackburn, *Journal of Applied Physics* **52**(4), 2944–81.
- [6] Norio Mochida, Takao Sekiya, Atsushi Ohtsuka, Mamoru Tonokawa, *Journal of the Ceramic Society of Japan* **96**(1118), 973 (1988).
- [7] Petr Mošner, Kateřina Vosejpková, Ladislav Koudelka. *Thermochimica acta* **522**(1-2), 155011).
- [8] Jitka Ozdanova, Helena Ticha, Ladislav Tichy. *Optical Materials* **32**(9), 950 (2010).
- [9] S. Rada, M. Culea, E. Culea, *The Journal of Physical Chemistry A* **112**(44), 11251 (2008).
- [10] A. H. Khafagy, A. A. El-Adawy, A. A. Higazy, S. El-Rabaie, A. S. Eid, *Journal of Non-Crystalline Solids* **354**(14), 1460 (2008).
- [11] N. S. Tagiara, D. Palles, E. D. Simandiras, V. Psycharis, A. Kyritsis, E. I. Kamitsos, *Journal of Non-Crystalline Solids* **457**, 116 (2017).
- [12] J. Wasylak, M. Reben, *Physics and Chemistry of Glasses-European Journal of Glass Science and Technology Part B* **48**(4), 246 (2007).
- [13] El Sayed, S. Yousef, *Journal of Physics D: Applied Physics* **38**(21), 3970 (2005).
- [14] Naoyuki Kitamura, Kohei Fukumi, Junichi Nakamura, Tatsuo Hidaka, Takurou Ikeda, Hidekazu Hashima, Junji Nishii, *Journal of Non-Crystalline Solids* **357**(3), 1188 (2011).
- [15] A. Miguel, R. Morea, J. Gonzalo, M. A. Arriandiaga, J. Fernandez, R. Balda, *Journal of Luminescence* **140**, 38 (2013).
- [16] W. A. G. H. Akshatha, Y. Raviprakash, M. P. Ajithkumar, V. Upadhyaya, Sudha D. Kamath, *Transactions of Nonferrous Metals Society of China* **25**(4), 1185 (2015).
- [17] U. B. Chanshetti, A. Shelke, S. M. Jadhav, S. G. Shankarwar, T. K. Chondhekar, A. G. Shankarwar, V. Sudarsan, M. S. Jogad, *Facta universitatis-series: Physics, Chemistry and Technology* **9**(1), 29 (2011).
- [18] S. Likityvanichkul, Lacourse, J. Mater. Sci. **30**, 6151 (1995).
- [19] R. El-Mallawany, I. Z. Hager, *Journal of Materials Science* **37**, 3291 (2002).
- [20] M. A. Sidkey, M. S. Gaafar, *Physica B* **348**, 46 (2004).
- [21] N. Elkhoshkhany, Eslam Syala, *Journal of Non-Crystalline Solids* **486**, 19 (2018).
- [22] M. M. Elokr, Y. M. Abou Deif, *J. Mol. Struct.* **1108**, (2016) 257.
- [23] Maria Lasocka, *Mater. Sci. Eng.* **23**, 173 (1976).
- [24] Haiwei Yin, Lei Li, Yinyao Liu, Lili Hu, Huidan Zeng, Guorong Chen, *Ceram. Int.* **43**, 3556 (2017).
- [25] R. El-Mallawany, A. Abousehly, A. El-Rahamani, E. Yousef, *Phys. Status Solidi A* **163**, 377 (1997).
- [26] M. L. Oveçoğlu, G. Özen, B. Demirata, A. Genç, *J. Eur. Ceram. Soc.* **21**, 177 (2001).
- [27] E. A. Mohamed, F. Ahmad, K. A. Aly, *Journal of Alloys and Compounds* **538**, 230 (2012).
- [28] V. Kamalaker, G. Upender, Ch. Ramesh, V. Chandra Mouli, *Spectrochimica Acta Part A: Molecular and Biomolecular Spectroscopy* **89**, 149 (2012).
- [29] Azlan Muhammad Noorazlan, Halimah Mohamed Kamari, Siti Shafinas Zulkefly, Daud W. Mohamad, *Journal of Nanomaterials* **2013**, 168 (2013).
- [30] V. Kamalaker, G. Upender, M. Prasad, V. Chandra Mouli, *Infrared, ESR and optical absorption studies of Cu²⁺ ions doped in TeO₂-ZnO-NaF glass system*, (2010).
- [31] N. Elkhoshkhany, Samir Y. Marzouk, Shima Shahin, *Journal of Non-Crystalline Solids* **472**, 39 (2017).
- [32] Samir Y. Marzouk, Roshdi Seoudi, Doaa A. Said, Mai S. Mabrouk, *Optical Materials* **35**(12), 2077 (2013).
- [33] A. E. Al-Salami, Mario Hotzel. *Bulletin of Materials Science* **35**(6), 961 (2012).
- [34] Vesselin Dimitrov, Sumio Sakka, *Journal of Applied Physics* **79**(3), 1736 (1996).
- [35] Halimah, M. K., M. F. Faznny, M. N. Azlan, H. A. A. Sidek, *Results in Physics* **7**, 581 (2017).
- [36] Petr Mošner, Kateřina Vosejpková, Ladislav Koudelka, Lionel Montagne, Bertrand Revel, *Journal of Non-Crystalline Solids* **357**(14), 2648 (2011).
- [37] E. K. Abdel-Khalek, Ibraheem Othman Ali, *Journal of Non-Crystalline Solids* **390**, 31 (2014).

- [38] N. Elkhoshkhany, R. El-Mallawany, Eslam Syala, *Ceramics International* **42**(16), 19218 (2016).
- [39] G. Lakshminarayana, Kawa M. Kaky, S. O. Baki, A. Lira, Priyanka Nayar, I. V. Kityk, M. A. Mahdi, *Journal of Alloys and Compounds* **690**, 799 (2017).
- [40] Keiji Kobayashi, Hideyuki Sasaki, *Journal of the European Ceramic Society* **19**(5), 637 (1999).
- [41] Shaaban M.Salem, *Journal of Non-Crystalline Solids* **358**(11), 1410 (2012).
- [42] Shaik Kareem Ahmmad, M. A. Samee, S. M. Taqiullah, Syed Rahman, *Journal of Taibah University for Science* **10**(3), 329 (2016).
- [43] Gwenn Le Saout, Patrick Simon, Franck Fayon, Annie Blin, Yann Vaills, *Journal of Raman Spectroscopy* **33**(9), 740 (2002).
- [44] N. Elkhoshkhany, M. A. Khatab, Marwa A. Kabary, *Ceramics International* **44**(3), 2789 (2018).
- [45] Petr Mošner, Kateřina Vosejpková, Ladislav Koudelka, Lionel Montagne, Bertrand Revel. *Materials Chemistry and Physics* **124**(1), 732 (2010).